Max-Planck-Institut
für Meteorologie

REPORT No. 156

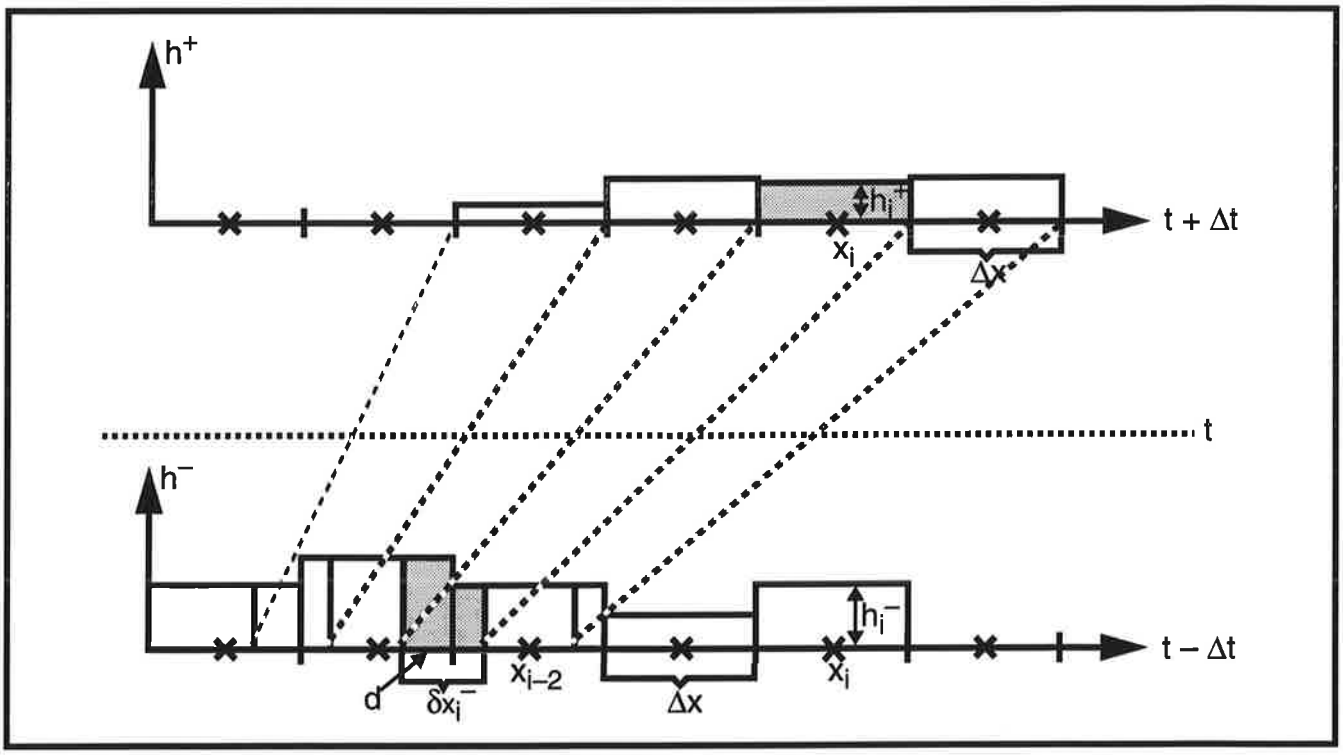

THE IMPLEMENTATION OF THE SEMI-IMPLICIT SCHEME IN CELL-INTEGRATED SEMI-LAGRANGIAN MODELS

by

BENNERT MACHENHAUER • MARKUS OLK

HAMBURG, February 1995

AUTHORS:

Bennert Machenhauer — Max-Planck-Institut für Meteorologie
Hamburg, Germany

Markus Olk — Max-Planck-Institut für Meteorologie
Hamburg, Germany

MAX-PLANCK-INSTITUT
FÜR METEOROLOGIE
BUNDESSTRASSE 55
D-20146 HAMBURG
F.R. GERMANY

Tel.: +49 - (0)40 - 411 73 - 0
Telefax: +49 - (0)40 - 411 73 - 298
E-Mail: <name>@dkrz.d400.de

The implementation of the semi-implicit scheme in cell-integrated semi-Lagrangian models

by

Bennert Machenhauer and Markus Olk
Max-Planck-Institute for Meteorology, Hamburg, Germany

ISSN 0937 – 1060

Abstract

The cell-integrated semi-Lagrangian method, in which trajectories from the corner points of a grid cell define its extent at a previous time, may be applied to a set of equations on Lagrangian form derived from the complete set of primitive equations to construct a numerical model which conserves exactly the discrete forms of the global integrals constraints of mass, momentum, entrophy and total energy. Due to the fulfilment of these integral constraints one should expect the numerical model to be absolutely stable. Experiments with a simple one-dimensional shallow water model show, however, that a time step dependent instability develops when a CFL criterion for gravity waves is exceeded. Analysis of experiments with one-dimensional shallow water models unveil the mechanism of the instability. Using again for simplicity one-dimensional models a main achievement is a successful implementation of the semi-implicit time stepping scheme in the cell-integrated models.

1. Introduction

The accuracy of atmospheric numerical models has steadily improved with enhanced resolution and improvements in physical parameterisation schemes. This increase of accuracy, which has taken place for the relatively high resolution weather prediction models as well as for the lower resolution climate models, has been made possible due to the steadily growing computer power and due to the introduction of more efficient numerical techniques. One such numerical technique was the semi-implicit time stepping scheme, which was introduced by André Robert (Robert, 1969, Kwizak and Robert, 1971) and is used now in most atmospheric models to eliminate the Courant-Friedrichs-Levy (CFL) time step restriction due to gravity waves. In semi-implicit models typically a six time larger time step than in the former explicit models can be used without loss of accuracy. The time step in the usual Eulerian semi-implicit models is limited only by the advective CFL restriction. Another important new technique, also introduced in meteorological applications by Robert (1981, 1982), is a semi-Lagrangian treatment of advection offering a potential further increased efficiency by elimination of the advective CFL time-step restriction. In principle, the time step in a combined semi-implicit semi-Lagrangian model can be chosen based on accuracy considerations. As developers of physical parameterisations are uncomfortable applying their schemes over time steps exceeding one hour (Williamson and Olson, 1994), this may put an upper bound to the time steps which can be used in practice. Significant computational savings can however be obtained in many applications, even within this limit.

The semi-Lagrangian advection offers additional advantages beyond the longer time-step. It gives minimal phase error, minimizes computational dispersion, can handle sharp discontinuities and furthermore desirable properties such as monotonicity or, more generally, shape preservation may easily be incorporated.

A disadvantage is that the smallest scales resolved may be damped more by semi-Lagrangian methods than by some Eulerian methods. However, this seems not to be a serious issue as it can be counteracted by a reduction or elimination of horizontal diffusion. A more serious disadvantage of semi-Lagrangian schemes today is that they do not formally conserve integral invariants as total mass or total energy. This may not be a problem in weather forecasting applications. For long simulations in climate applications, however, lack of conservation might have serious consequences. The total mass, in particular, has been found to drift significantly if no corrections are applied during longer integrations. Moorthi et al. (1994) report that the global mean surface pressure increased monotonously over a seventeen-month

integration period. The rate of increase varied and at the end of this seventeen-month period it had increased 34 hPa from its initial value. In another case, reported by Machenhauer (1994), a three-month test integration with an early version of the ECMWF operational semi-implicit semi-Lagrangian model resulted in a systematic loss of mass corresponding to 4.5 hPa. Obviously in these cases errors in the prediction equation for surface pressure are accumulating. The mecanism(s) leading to these errors are not known and we can detect only the error in the global mean surface pressure field. Therefore, we know nothing about the three dimensional structure of the errors in the mass field. It seems likely, however, that the accumulating large errors in the mean surface pressure are accompanied by pressure errors locally which are even larger and which may be systematically correlated with the pressure pattern. If such a correlation exists the internal dynamics of the model may be affected significantly. We do not know if this is the case, but it seems possible, and if it is the case the non-conservation is a symptom of some, perhaps more serious systematic errors.

Conservation of total mass may be obtained by a "mass-fixer" which after each time step restores the mean surface pressure to its initial value. Such a mass-fixer was tested by Moorthi et al. (1994) who repeated the above mentioned seventeen-month integration restoring after each time step the mean surface pressure by multiplying everywhere the preliminary calculated surface pressure by a constant factor equal to the ratio between the initial mean value and the preliminary mean value. This mass-fixer is similar to that used by (Williamson and Olson, 1994), except that they allow for variations in the total mass of water vapour. By this form of the mass-fixer the horizontal pressure gradient is not affected by a restoration and the effect on the internal dynamics is therefore minimized. When comparing seasonally averaged fields from the above mentioned seventeen-month integrations with and without mass restoration Moorthi et al. (1994) found no significant differences. Thus, with this type of mass-fixer the restoration does not seem to affect significantly the simulated climate. This result is not so surprising as the fixer as mentioned above was designed to have minimal effect on the dynamics. The restoration each time step with the same factor everywhere is of course completely arbitrary and most likely the geographical distribution of the corrections is wrong. Recently Gravel and Staniforth (1993) have presented an alternative mass-fix procedure where the restoration of the mean pressure is made only in some specially selected points. They describe their mass-fix procedure as an extension to the shallow water equations of an algorithm introduced by Priestly (1993). The mass-fixer builds upon a mass conservation constraint imposed in the quasi-monotone semi-Lagrangian scheme of Bermejo and Staniforth

(1992). This scheme in turn build on the monotonicity constraint that an interpolated value must lay between the minimum and maximum value of the four neighbouring points. In the mass-fix procedure of Gravel and Staniforth (1993) the values are preliminary adjusted toward linear interpolated values at points at which a cubic interpolation violates the monotonicity constraint. These adjustments are kept as small as possible (at many points they are zero). Then the total mass is restored to its initial value by adjusting further toward the linear solution, but only in those points where such an adjustment changes the mass in the right direction and do so without violating the monotonicity constraint. Thus, the corrections applied in order to achieve conservation of mass are made only in some of those points where the monotonicity constraint is violated. Gravel and Staniforth (1993) argue that the interpolation is likely to introduce the errors that cause the lack of conservation in areas of strong gradients and that the points where they make the corrections are exactly such points. A great deal of arbitrariness is, however, still present in their procedure with regard firstly to the magnitude of correction in each point (kind of equipartition among the points chosen) and secondly by choosing not to do any mass restoring corrections in those points in which the preliminary correction to fulfil monotonicity goes in the "wrong" direction.

In the present paper we will advocate for a different approach towards incorporating conservation principles within the semi-Lagrangian framework. Namely to use special forms of the meteorological equations and special numerical schemes designed to conserve integral invariants exactly. Such a system based upon the full set of primitive equations was set up in Machenhauer (1994). Each of the prognostic equations in the system was written on the form

$$\frac{d}{dt}(X\delta M) = F_X + \delta M S_X \tag{1}$$

where δM is the mass of an infinitesimal particle moving with the flow, X is unity or the mean value over the particle of a conservative variable, F_X is a flux and/or pressure terms working at the surface of the parcel and S_X is a source term working inside the parcel. When X is unity ($X \equiv 1$), equation (1) is the continuity equation for which both right hand terms are zero. In the remaining equations of the system, X is specific total energy, specific angular momentum, specific entrophy, specific humidity or specific liquid water. In the semi-Lagrangian discretization of (1) grid point values of X are assumed to be mean values over the surrounding grid cell. As the moving parcel in (1) we consider the mass of air which at the end of a time step is ending up in a grid cell. It is traced back in time using trajectories from the corner points of the

grid cell. With a consistent evaluation of the flux terms F_X in neighbouring grid cells and a conservative remapping of X at the previous time level the integral invariants valid for (1) are maintained also for the discrete form of the system. A model based on equations of the form (1) and in the finite-difference form as indicated above will be called a cell-integrated semi-Lagrangian model.

In Machenhauer (1994) we speculated that perhaps due to the conservation properties of such a model it might be absolutely stable even with an explicit time-stepping scheme. In Section 3 we shall see, however, that experiments with simple one-dimensional versions, which are derived in Section 2, show that even such a model becomes unstable when the time step exceeds the critical value determined by the CFL criterion for gravity waves. The most unstable short waves are found to grow in amplitude even though total mass and total momentum or total mass and total energy are conserved exactly. When the amplitude has become large the trajectories begin to cross in some points which at once causes a break down of the conservation properties and subsequently leads to an explosion.

In order for a cell-integrated semi-Lagrangian model to be able to compete with traditional semi-Lagrangian models it is essential that a semi-implicit time-stepping scheme can be introduced in the cell-integrated system. The main purpose of the present paper is to show that this can be accomplished successfully. This is done in Section 4, again using simple one-dimensional models. Finally, a summary and conclusions are given in Section 5.

After the design of the cell-integrated semi-Lagrangian system considered here it was realized that a somewhat similar system had been developed for the Navier-Stokes equations by Hirt et al. (1974) and had been applied to hydrodynamical problems. Here a more general application to the complete system of meteorological equations is considered. Furthermore we use a semi-Lagrangian approach with a remapping every time step, whereas in the Hirt et al. (1974) either an Eulerian or a fully Lagrangian approach for extended periods were used. Finally in order to be able to use larger time steps in the cell-integrated semi-Lagrangian system we introduce a semi-implicit time-stepping scheme whereas Hirt et al. (1974) introduced an iterative procedure to adjust pressure gradient forces.

More similar in all respects to the cell-integrated scheme proposed here are the advection schemes introduced and tested by Rancic (1992) and Laprise and Planté (1995). Although we did not know their works when our scheme was initially developed, the cell-integrated model system we propose may be considered as an extension to the complete system of the meteorological equations of the scheme developed by Rancic (1992) and the similar one

developed independently by Laprise and Planté (1995).

2. One-dimensional explicit models

We shall do experiments with simple one-dimensional versions of the cell-integrated semi-Lagrangian model. In this section we shall derive model equations based on leap-frog time differencing.

The shallow water continuity and velocity equations are

$$\frac{dh}{dt} + h\frac{\partial u}{\partial x} = 0 \tag{2}$$

$$\frac{du}{dt} + g\frac{\partial h}{\partial x} = 0 \tag{3}$$

where u is velocity, h height, x distance, t time and g gravity. We assume a periodic domain $0 \leq x \leq L$. Two different versions may be set up: A version in which mass and energy are conserved and a version in which mass and momentum are conserved. We shall call them the energy and the momentum system, respectively. We shall consider both versions since both are simplified versions of the complete three-dimensional system.

Let us consider at first the momentum system. From (2) and (3) we derive the momentum equation

$$\frac{d}{dt}(uh) + uh\frac{\partial u}{\partial x} + gh\frac{\partial h}{\partial x} = 0. \tag{4}$$

In (2) and (4) we substitute the Lagrangian expression for divergence

$$\frac{\partial u}{\partial x} = \frac{1}{\delta x}\frac{d}{dt}(\delta x) \tag{5}$$

where δx is an infinitesimal length interval. We thereby bring the momentum and continuity equation on the form (1):

$$\frac{d}{dt}(h\delta x) = 0 \tag{6a}$$

$$\frac{d}{dt}(uh\delta x) + g\delta x\frac{\partial}{\partial x}(\frac{1}{2}h^2) = 0 \tag{6b}$$

The finite difference approximation of these equations is based on trajectories that are ending up at time $t+\Delta t$ at the cell boundaries, i. e. at the mid points between gridpoints. Such trajec-

tories are illustrated in Figure 1. We chose a three-level leap-frog scheme with timestep Δt and a uniform grid with gridlength Δx. The trajectories are then determined from velocities at time $t=n\Delta t$ using the usual iterative procedure to find the departure points at time $t-\Delta t$ which are given by

$$x_{j+1/2-2\alpha(j)} = x_{j+1/2} - 2\Delta t u^{n}_{j+1/2-\alpha(j)} \tag{7}$$

where $x_j=j\Delta x$ and consequently $2\alpha(j)$ is the distance in units of Δx between the departure point and the arrival point of the trajectory ending at $x_{j+1/2}$. Here the velocities are determined by cubic interpolation. The form chosen for the finite-difference analogue of (6a) is

$$h_j^{n+1}\Delta x = \bar{h}_j^{-}\delta x_j^{-} \tag{8}$$

where

$$\delta x_j^{-} = x^{n-1}_{j+1/2-2\alpha(j)} - x^{n-1}_{j-1/2-2\alpha(j-1)} = \Delta x - 2\Delta t \delta u_j^{0} \tag{9}$$

$$\text{with} \quad \delta u_j^{0} = u^{n}_{j+1/2-\alpha(j)} - u^{n}_{j-1/2-\alpha(j-1)}$$

and $\bar{h}_j^{-}$ is the integral mean value of h^{n-1} over the interval δx_j^{-}:

$$\bar{h}_j^{-} = \frac{1}{\delta x_j^{-}} \int_A^B h^{n-1}(x)\,dx \tag{10}$$

with $A = x^{n-1}_{j-1/2-2\alpha(j-1)}$ and $B = x^{n-1}_{j+1/2-2\alpha(j)}$. In order to determine $\bar{h}_j^{-}$ the function $h^{n-1}(x)$ must be defined from the gridpoint values h_j^{n-1}. As mentioned in the introduction each of the grid point values are assumed to be equal to the mean value over its grid cell, i.e.

$$h_j^{n} = \frac{1}{\Delta x} \int_{x_{j-1/2}}^{x_{j+1/2}} h^{n}(x)\,dx. \tag{11}$$

The most simple definition of $h^{n-1}(x)$ consistent with this is to assume $h^{n-1}(x)$ in each grid cell to be piecewice constant equal to the grid point value, that is

$$h^{n}(x) = h_j^{n} \quad \text{for} \quad x_{j-1/2} \le x \le x_{j+1/2}, \tag{12}$$

as indicated in Figure 1. The integral in (10) is then easily evaluated by a simple "length-weighted" mean, at the grid point x_j in the figure for instance by

$$\delta x_j^- \overline{h_j}^- = d h_{j-3}^{n-1} + (\delta x_j^- - d)\, h_{j-2}^{n-1} \tag{13}$$

where d is a distance defined in the figure. It is obvious that by this procedure we obtain

$$\sum_j h_j^{n+1} \Delta x = \sum_j \overline{h_j}^- \delta x_j^- = \sum_j h_j^{n-1} \Delta x \tag{14}$$

which means exact conservation of total mass. The first equality in (14) follows from (8) and the last one from (10) and (11). Calculation of mean values over a "new" set of grid cells δx_j^-, from the grid point values, h_j^{n-1}, in an "old" grid as we do when using (10), is called a "remapping". If the remapping is satisfying the last equality in (14) it is termed "conservative". The condition for a conservative remapping, and thereby exact conservation of total mass, is that the $h^n(x)$ used in (10) must satisfy (11). The choice (12) is the most simple possibility. It is easy to show that with this choice and a constant wind (8) and (9) becomes equal to an upstream in space, forward in time first order advection scheme, a monotone but excessively damping scheme. Instead of the piecewice constant functions (12) a piecewice higher order polynomial, constrained to satisfy (11), may be used. The piecewice parabolic functions used by Rancic (1992) and Laprise and Planté (1995) seem to constitute a proper balance between increased accuracy and increased complexity. For simplicity we shall use the piecewice constant functions (12) also because the advection process is of secondary importance in the experiments to be performed here.

The discrete form of the momentum equation (6b) is

$$(uh)_j^{n+1} \Delta x = \overline{(uh)_j}^- \delta x_j^- - \Delta t g \delta (h^2)_j^0 \tag{15}$$

where

$$\delta (h^2)_j^0 = (h^n_{j+1/2-\alpha(j)})^2 - (h^n_{j-1/2-\alpha(j-1)})^2 \tag{16}$$

and where $\overline{(uh)_j}^-$ is defined as an integral mean value analogous to (10) which is computed assuming that also $(uh)^{n-1}(x)$ is piecewice constant in the grid cells. For the grid point x_j in the

figure for instance it becomes

$$\overline{(uh)_j}^{-}\delta x_j^{-} = (d\,(uh)_{j-3}^{n-1} + (\delta x_j^{-} - d)\,(uh)_{j-2}^{n-1})\,. \tag{17}$$

The values of h at the mid points of the trajectories to be used in (16) are determined from the grid points by cubic interpolation.

The total momentum is conserved exactly because

$$\sum_j (uh)_j^{n+1}\Delta x = \sum_j \overline{(uh)_j}^{-}\delta x_j^{-} = \sum_j (uh)_j^{n-1}\Delta x \tag{18}$$

where the first equality follows from (15) and the last one follows from the conservative remapping of $(uh)^{n-1}$.

The prognostic equations for the momentum system, equation (8) and (15), have now been derived and we proceed with the derivation of the energy equation. We define the total energy as

$$E = \frac{1}{2}u^2h + \frac{1}{2}gh^2. \tag{19}$$

From the original system (2) and (3) we derive the energy equation

$$\frac{dE}{dt} + E\frac{\partial u}{\partial x} + \frac{\partial}{\partial x}(\frac{1}{2}gh^2u) = 0 \tag{20}$$

which, after substitution of (5), is brought on the form (1):

$$\frac{d}{dt}(E\delta x) + \delta x\frac{\partial}{\partial x}(\frac{1}{2}gh^2u) = 0. \tag{21}$$

We approximate this equation as

$$E_j^{n+1}\Delta x = \overline{E_j}^{-}\delta x_j^{-} - g\Delta t\delta(h^2u)_j^0 \tag{22}$$

where

$$\delta(h^2u)_j^0 = (h^n_{j+1/2-\alpha(j)})^2 u^n_{j+1/2-\alpha(j)} - (h^n_{j-1/2-\alpha(j-1)})^2 u^n_{j-1/2-\alpha(j-1)} \tag{23}$$

and, with similar assumptions as in the momentum system, $\overline{E_j}^{-}$ becomes a length-weighted

mean value. For the case shown in the figure we obtain

$$\overline{E_j}^{-}\delta x_j^{-} = dE_{j-3}^{n-1} + (\delta x_j^{-} - d)\,E_{j-2}^{n-1}. \tag{24}$$

As for the momentum equation we use cubic interpolation in (23). From (22) and the conservative remapping of E^{n-1} we get exact conservation of Energy:

$$\sum_j E_j^{n+1}\Delta x = \sum_j \overline{E_j}^{-}\delta x_j^{-} = \sum_j E_j^{n-1}\Delta x. \tag{25}$$

When using the momentum system the time stepping procedure is straight forward. In each time step we compute at first h^{n+1} using (8) and then we use (15) to compute u_j^{n+1}, that is

$$u_j^{n+1} = \frac{(uh)_j^{n+1}}{h_j^{n+1}}.$$

For the energy system it becomes slightly more complicated. Again we compute at first h^{n+1} using (8). To obtain u_j^{n+1} we then use (22) to get E_j^{n+1} which gives

$$u_j^{n+1} = \pm\sqrt{2E_j^{n+1}/h_j^{n+1} - gh_j^{n+1}}. \tag{26}$$

Thus, we have to choose between the plus and minus sign in (26). Normally we choose the same sign as $\overline{(uh)_j}^{-}$ determined from (17). It may happen, however, that the radicant in (26) becomes negative which means that the kinetic energy at time t+Δt had become negative. This will happen in grid cells which at the start of the time step have a numerically small velocity and are being decelerated sufficiently enough during the time step to change its direction of movement. The kinetic energy of such a cell should go to zero and then increase again. Assuming that the kinetic energy $E_{kin}=1/2\ u^2h$ is varying linearly with time, as illustrated in Figure 2, this may be simulated approximately simply by changing the sign of the predicted kinetic energy of every cell j for which it has become negative. As thereby the total energy is increased by an amount of $2\ |(E_{kin})_j^{n+1}|$ we reduce the predicted kinetic energy of the two neighbouring grid cells by an amount of $|(E_{kin})_j^{n+1}|$ each. (If one or two of the neighbours thereby get negative energy the same procedure is used in these points). At points where the sign of the kinetic energy has been changed we choose the opposite sign of that of $\overline{(uh)_j}^{-}$ in

(26). By this procedure we preserve conservation of total energy and "allow" particles to change the sign of their velocities within a time step. Normally, with a realistic size of Δt and realistic atmospheric flows it should be few points if any where corrections of kinetic energy are needed. Except in unstable integrations just before the model "explodes" no corrections of kinetic energy were made in the experiments reported on later.

As for other semi-Lagrangian schemes the present scheme breaks down when any of the trajectories cross each other or in other words when any of the δx_j^- becomes negative. Using (9) it is easily shown that this condition puts a limit to the magnitude of the divergence of the velocity field which determines the trajectories, or rather to the finite difference approximation which we use for this divergence. The condition becomes

$$\frac{\partial u}{\partial x} \approx \frac{\delta u_j^0}{\Delta x/2} \leq \frac{1}{\Delta t}. \tag{27}$$

3. Stability of explicit cell-integrated models

To investigate the stability of the cell-integrated models designed above some experiments were carried out. In these experiments and those reported in the following section we used the following set up:

- A periodic domain of 64 grid points and a grid length of Δx=100 km.
- Initial fields defined as follows:

$$u = U + u_0 \sin\left(\frac{2\pi}{L}x\right) \tag{28a}$$

$$h = H + h_0 \sin\left(\frac{2\pi}{L}x\right) \tag{28b}$$

where U=10 m/s, H=8000 m, L=6400 km, u_0=0.5 m/s and $h_0 = u_0\sqrt{H/g} \approx 14.28m$.

These are the initial fields of a harmonic solution with maximum wavelength to the linearized system corresponding to (2) and (3). It is one of the two gravity wave solutions with this wave length. Its phase speed is

$$c_g = U + \sqrt{gH} \approx 290.14 m/s \tag{29}$$

- A so-called smooth starting procedure used to compute fields at t=Δt.

In the present experiments with explicit time stepping the fields at t=Δt were computed by an initial Euler time step over Δt/2 followed by a leap-frog step centred at t=Δt/2. In the Euler step the trajectories were computed using velocities valid at t=0.

The results obtained with the cell-integrated models will be compared with those of a traditional model based on the original velocity and continuity equations (2) and (3), in the following referred to as the velocity system. The prediction equations for this model are

$$u_j^{n+1} = u_{j-2\alpha'(j)}^{n-1} - \frac{\Delta t g}{\Delta x} (\delta_{2\Delta x}(h))_{j-\alpha'(j)}^{n} \tag{30}$$

$$h_j^{n+1} = h_{j-2\alpha'(j)}^{n-1} - \frac{\Delta t}{\Delta x} (h\delta_{2\Delta x}(u))_{j-\alpha'(j)}^{n} \tag{31}$$

where $2\alpha'(j)$ is the distance in units of Δx between departure and arrival point for the trajectory ending at gridpoint x_j. $\delta_{2\Delta x}(h)$ is a finite difference centred over 2Δx. It is computed in grid points and $(\delta_{2\Delta x}(h))_{j-\alpha'(j)}^{n}$ is a value obtained from these by interpolation to the mid points of the trajectories. As in the cell-integrated model cubic interpolation is used to compute the velocities needed for the trajectory computations and to compute the terms on the right hand sides of (30) and (31).

Using at first a time step Δt=100 s the two cell-integrated models and the traditional model were integrated for 1100 time steps or 30.5 hours. During this period the linear solution is moving slightly less than 5 times through the domain. The three numerical solutions at the end of the integration period are plotted together with the linear solution on top of each other in Figure 3. Only the height field is shown. The solutions of the two cell-integrated models, i.e. the dashed and dot-dashed curves in the figure, can not be distinguished. Compared to the linear solution their amplitudes have decreased by about 5% which can be attributed almost exclusively to the smoothing due to the length weighting, i.e. the expression (10) with $h^{n-1}(x)$ being piecewice constant in the grid cells, as we choose for simplicity. As mentioned above, by a more sophisticated choice this damping can be reduced. A similar damping is not visible in the traditional model solution. The cell-integrated model solutions deviate slightly from a sine shape being steeper between the maximum and minimum than between minimum and the

maximum. We see the same deformation in the solution of the traditional model, which may indicate that it is a true nonlinear effect. As seen by crossing points at the 8000 m line the solutions are retarded slightly compared to the true linear solution. This retardation is largest for the traditional model solution.

A difference between the cell-integrated models solutions and the traditional model solution is, of course, that the former conserves mass and energy or mass and momentum exactly whereas the latter does not. This was verified in practice by integrating the three models for 62.5 days ($5.4 \cdot 10^6$ time steps). In these extended integrations a week Robert-Asselin time filter with a coefficient of 0.005 were applied to the prognostic variables in order to avoid separation between values at even and odd time steps. The time filter is not affecting the conservation properties of the cell-integrated models. Due to the time filter and other numerical damping mechanisms the initial perturbations were completely damped out at the end of the integration period in all three model runs. Although our models based on the simple one dimensional shallow water equations are well suited for the main objectives of the present study they are unrealistic as models of the atmosphere in most respects. The changes of mass, momentum and energy we find in the extended integrations are therefore not of particular interest and will not be listed here.

In order to test the stability of the cell-integrated models integrations with larger Δt were performed. From integrations with a time step Δt=300 s the resulting height fields are shown in Figure 4, for the energy system after 64 time steps and for the momentum system after 70 time steps. Obviously in both systems a beginning instability of waves with a mean wave length around $3\Delta x$ to $4\Delta x$ is developing. A few time steps later the models "explode". This instability develops in spite of the exact conservation of total mass and total energy or total mass and total momentum in the models. What happens is the following: The short waves are growing in amplitude even though mass and momentum/energy are conserved exactly. When the amplitude has become large enough the critical value for divergence, given by (27), is ex-ceeded locally, which causes the trajectories to cross in some cells. As a result of these crossings the conservation properties are no longer valid and immediately we see a very rapid increase in the quantities that were formerly conserved.

In order to demonstrate an equivalence between the growth of short waves in the cell-integrated systems on one hand and CFL-type instability of a corresponding linearized system on the other hand we have made a stability analysis of such a linearized system. The discrete continuity equation (8) may be linearized as follows. Using (9) we may write (8) as

$$h_j^{n+1}\Delta x = \overline{h_j}^{-}\delta x_j^{-} = \overline{h_j}^{-}(\Delta x - 2\Delta t\delta u_j^0) = \overline{h_j}^{-}\Delta x - 2\Delta t\overline{h_j}^{-}\delta u_j^0 .$$

When $h_j=h'_j+H$ and $u_j=u'_j+U$ are inserted and second order terms in perturbation quantities are dropped we get the linearized continuity equation

$$h_j'^{n+1} = \overline{h'_j}^{-} - 2\Delta tH\frac{\delta u_j'^0}{\Delta x}, \tag{32}$$

similarly for the momentum equation (15) we obtain

$$(uh)_j^{n+1}\Delta x = \overline{(uh)_j}^{-}\delta x_j^{-} - 2\Delta t\delta(h^2)_j^0 .$$

Using again (9) and the following approximations

$$(uh)_j^{n+1} = u_j^{n+1}h_j^{n+1} \cong Uh_j'^{n+1} + Hu_j'^{n+1} + UH$$

$$\overline{(uh)_j}^{-} \cong U\overline{h'_j}^{-} + H\overline{u'_j}^{-} + UH$$

$$(h^2)_j^0 \cong 2gHh_j'^n + gH^2$$

where second order terms in perturbed variables have been dropped, this equation becomes

$$\left(u_j'^{n+1} - \overline{u'_j}^{-} + 2\Delta tg\frac{\delta h_j'^0}{\Delta x}\right)H + \left(h_j'^{n+1} - \overline{h'_j}^{-} + 2\Delta tH\frac{\delta u_j'^0}{\Delta x}\right)U = 0$$

which when (32) is used gives

$$u_j'^{n+1} = \overline{u'_j}^{-} - 2\Delta tg\frac{\delta h_j'^0}{\Delta x}. \tag{33}$$

Dropping the perturbation marks the linearized system is

$$h_j^{n+1} - \overline{h_j}^{-} + 2\Delta tH\frac{\delta u_j^0}{\Delta x} = 0 \tag{34a}$$

$$u_j^{n+1} - \overline{u_j}^{-} + 2\Delta tg\frac{\delta h_j^0}{\Delta x} = 0. \tag{34b}$$

By a similar procedure the linearized version of the energy system may be derived. It turns out to be identical to the above system.

Using a constant basic stream velocity U in the computation of trajectories these become parallel, i.e. δx_j^- becomes constant equal to Δx and a length-weighted quantity is then simply obtained as a linear interpolation between two grid point values. For the height for instance

$$\overline{h_j}^- = (1-\mu)\, h_J^{n-1} - \mu h_{J-1}^{n-1} \tag{35}$$

where

$$\mu = \frac{2\Delta t U}{\Delta x} - INT\left(\frac{2\Delta t U}{\Delta x}\right) \tag{36}$$

and

$$J = j - INT\left(\frac{2\Delta t U}{\Delta x}\right). \tag{37}$$

Here INT(a) is defined as the largest integer which is ≤ a. In the present case with U=10 m/s, Δx=100 km and Δt of the order 100 s, INT(2ΔtU/Δx)=0 and $\mu << 1$. The evaluation of the last term in each of the equations (34a,34b) involves interpolations of u^n and h^n to the mid points of the trajectories. These points lay at a distance $\mu\Delta x/2$ upstream from the mid points between the grid points. As $\mu << 1$ this distance is very small so we can neglect it which simplifies the formulation of the cubic interpolation. With this approximation equations (34a,34b) may be written

$$h_j^{n+1} - \left((1-\mu)\, h_j^{n-1} + \mu h_{j-1}^{n-1}\right) + \frac{2\Delta t H}{\Delta x}\left(\frac{5}{8}\left(u_{j+1}^n - u_{j-1}^n\right) - \frac{1}{16}\left(u_{j+2}^n - u_{j-2}^n\right)\right) = 0 \tag{38a}$$

$$u_j^{n+1} - \left((1-\mu)\, u_j^{n-1} + \mu u_{j-1}^{n-1}\right) + \frac{2\Delta t g}{\Delta x}\left(\frac{5}{8}\left(h_{j+1}^n - h_{j-1}^n\right) - \frac{1}{16}\left(h_{j+2}^n - h_{j-2}^n\right)\right) = 0 \tag{38b}$$

The condition for existence of harmonic solutions of the form

$$\begin{pmatrix} u_j \\ h_j \end{pmatrix}^n = \begin{pmatrix} u_k \\ h_k \end{pmatrix} e^{ik(j\Delta x - cn\Delta t)}$$

to the system (38) is found to be that

$$\sin^2(k(c-U)\Delta t) = \left(\frac{2\Delta t\sqrt{gh}}{\Delta x}F(k\Delta x)\right)^2 \tag{39}$$

where

$$F(k\Delta x) = \frac{5}{8}\sin(k\Delta x) - \frac{1}{16}\sin(2k\Delta x)\,.$$

In the deviation of (39) we have used again that μ is very small. From (39) we get the CFL condition of stability for the cell-integrated systems:

$$\frac{2\Delta t\sqrt{gh}}{\Delta x}F(k\Delta x) \le 1\,. \tag{40}$$

And the expression for the phase speeds of the two gravity wave solutions

$$c = U \pm \frac{1}{k\Delta t}arc\sin\left(\frac{2\Delta t\sqrt{gh}}{\Delta x}F(k\Delta x)\right) \tag{41}$$

valid when (40) is satisfied.

The function F(kΔx) and (c-U)/(c_g-U) are shown in Figures 5. The maximum value of F(kΔx) is 0.64 which occurs for kΔx=0.55π corresponding to a wave length of 3.6Δx. Inserting the maximum value of F(kΔx) in (40) gives the all over stability criterion

$$\Delta t \le \frac{\Delta x}{1.28\sqrt{gH}} \tag{42}$$

which for the present model set-up gives a maximum time step of 279 s. This agrees well with what we have found experimentally. In the results of our integrations with Δt=300 s, which are shown in Figure 4, we found growing waves with a wave length around 3Δx to 4Δx. This agrees well with the wave length of 3.6Δx found above for the most unstable wave in the linearized system. Finally, the experimentally found phase speeds agree very well with that determined from (41). These agreements show that the instability of the explicit cell-integrated semi-Lagrangian models that we found in the experiments can be identified as linear instability.

4. The semi-implicit formulation

If the cell-integrated semi-Lagrangian scheme shall be able to compete with traditional schemes in the context of climate modelling, formulations must be found which allow longer time steps, more reasonable in agreement with the time scale of large scale weather systems. In traditional models the most common way to eliminate the time step restriction due to linear instability of gravity waves is the use of a semi-implicit time stepping scheme. We shall see how that can be done also in cell-integrated semi-Lagrangian models, again for simplicity developed and tested for the one-dimensional models considered in the preceding sections.
We shall consider at first a traditional formulation corresponding to the explicit system (30) and (31). A semi-implicit system corresponding to this is obtained simply by averaging t+Δt and t−Δt values of the linear part of the divergence and pressure gradient terms along the trajectories instead of taking them at time t at the mid points of the trajectories. With a slightly simplified notation the resulting equations may be written

$$u^+ = u^+_{\exp} - \frac{\Delta t g}{2\Delta x}\left(\delta_{2\Delta x}h^+ + (\delta_{2\Delta x}h)^-_D - 2(\delta_{2\Delta x}h)^0_M\right) \tag{43a}$$

$$h^+ = h^+_{\exp} - \frac{\Delta t H}{2\Delta x}\left(\delta_{2\Delta x}u^+ + (\delta_{2\Delta x}u)^-_D - 2(\delta_{2\Delta x}u)^0_M\right) . \tag{43b}$$

Here "+", "−" and "0" stands for n+1, n−1 and n, respectively. "D" and "M" refer to departure and mid points and the index j has been dropped. $u^+_{\exp}$ and $h^+_{\exp}$ are the explicitly predicted values given by (30) and (31). We may write (43a,43b) as

$$u^+ = q_1 - \frac{\Delta t g}{2\Delta x}\delta_{2\Delta x}h^+ \tag{44a}$$

$$h^+ = q_2 - \frac{\Delta t H}{2\Delta x}\delta_{2\Delta x}u^+ . \tag{44b}$$

In q_1 and q_2 we have collected terms which depend on values at t−Δt and t. Applying the operator $\delta_{2\Delta x}$ on (44a) and substituting in (44b) gives

$$h^+ - \frac{\Delta t^2 g H}{(\Delta x)^2}\delta^2_{2\Delta x}(h^+) = q_2 - \frac{\Delta t H}{\Delta x}\delta_{2\Delta x}(q_1) \tag{45}$$

where $\delta^2_{2\Delta x} = \delta_{2\Delta x}\delta_{2\Delta x}$.

The Helmholtz equation (45) can be solved to give h^+ and then (44a) can be used to determine

u^+.

We shall try to set up a similar scheme for each of the cell-integrated systems. Two problems are encountered when trying to do that. The first problem that must be dealt with is the fact that the divergence, which we want to average over the time levels t+Δt and t−Δt, has been eliminated, i. e. by the use of (4). It is hidden in the trajectory computations as it may be seen from the last expression in (9):

$$\delta x_j^- = \Delta x - 2\Delta t \delta u_j^0$$

from which we may derive a finite difference expression for divergence at time level t

$$\left(\frac{\partial u}{\partial x}\right)_M^0 \approx \frac{\delta u_j^0}{\frac{1}{2}(\delta x_j^- + \Delta x)} = \frac{1}{\Delta t}\,\frac{\Delta x - \delta x_j^-}{\Delta x + \delta x_j^-}.$$

Thus, in the explicit system the divergence at time level t is determined by δx_j^- and therefore by the trajectory computations. In a semi-implicit system we would like in certain terms to use trajectories which were determined by winds that were averaged over time level t+Δt and t−Δt. That is not possible, however, as the velocities at time level t+Δt are not available at the beginning of a time step when the trajectory computations must be made. An iterative procedure might be a possibility but we rejected that as it would be too costly. We ended up by simply neglecting the problem using just explicitly computed trajectories in all terms of the equations.

The second problem we have to deal with is caused by the fact that one of the prognostic variables is a nonlinear quantity in the basic variables u and h. We solved this problem by a linearization of the nonlinear variable at time level t+Δt.

Let us consider at first the cell-integrated momentum system. The explicit continuity equation (8) may be written

$$h_{\exp}^+ \Delta x = \overline{h}_j^{-} \Delta x - 2\Delta t\,(H + \overline{h'}_j^{-})\,\delta u^0 \tag{46}$$

where (9) has been used. A corresponding semi-implicit equation is obtained by substituting $\frac{1}{2}(\delta u^+ + \delta u^-)$ for δu^0 in the linear part of the last term giving

$$h^+ = \overline{h}_j^{-} - \frac{2\Delta t}{\Delta x}\,\overline{h'}_j^{-}\delta u^0 + \frac{\Delta t H}{\Delta x}(\delta u^+ + \delta u^-) \tag{47}$$

where δu^- and δu^+ are defined analogous to δu^0 (see equation (9)), as the difference between the velocity at the right hand trajectory point and that at the left hand trajectory point at time level t–Δt and t+Δt, respectively. As mentioned above the trajectories referred to here are computed from velocities at time level t, as in the explicit scheme. The explicit momentum equation (15) may be written

$$(uh)^+_{\exp}\Delta x = \overline{(uh)_j}^-\Delta x - 2\Delta t\,(UH + \overline{(uh)'_j}^-)\,\delta u^0 - \Delta tg\,\delta(h'^2 + 2h'H)^0 \qquad (48)$$

and the corresponding semi-implicit one becomes

$$(uh)^+ = \overline{(uh)_j}^- - \frac{2\Delta t}{\Delta x}\overline{(uh)'_j}^-\delta u^0 - \frac{\Delta tg}{\Delta x}\delta(h'^2)^0 - \frac{\Delta tH}{\Delta x}(U(\delta u^+ + \delta u^-) + g(\delta h^+ + \delta h^-)) \qquad (49)$$

The next step is to write the two semi-implicit equations (47) and (49) as

$$h^+ = h^+_{\exp} - \frac{\Delta tH}{\Delta x}(\delta u^+ + \delta u^- - 2\delta u^0) \qquad (50a)$$

$$(uh)^+ = (uh)^+_{\exp} - \frac{\Delta tH}{\Delta x}(U(\delta u^+ + \delta u^- - 2\delta u^0) + g(\delta h^+ + \delta h^- - 2\delta h^0)) \qquad (50b)$$

where $h^+_{\exp}$ and $(uh)^+_{\exp}$ are values determined by the explicit equations (46) and (48), respectively. We note that equations (50) are similar in their form to the equations (43) of the traditional system. A difference is, however, that (50b) is nonlinear in the unknowns h^+ and u^+ whereas (43) were not. This prohibits us in deriving a Helmholtz equation analogous to (45), unless we carry out a linearization of (50b), we therefore do that as follows. The nonlinear term in (50b), the momentum at time level t+Δt, may be expanded as

$$(uh)^+ = ((U+u')(H+h'))^+ = (u'h')^+ + Hu'^+ + Uh^+.$$

In order to make it linear in h^+ and u'^+ we substitute $(u'h')^0$ for $(u'h')^+$ and get instead

$$(uh)^+ \approx ((u'h')^0 + Hu'^+ + Uh^+)\,. \qquad (51)$$

When (51) is inserted in (50b) it becomes after using (50a) and some algebra

$$u'^+ = \frac{1}{H}((uh)^+_{\exp} - Uh^+_{\exp} - (u'h')^0) - \frac{\Delta tg}{\Delta x}(\delta h^+ + \delta h^- - 2\delta h^0) \qquad (52)$$

which is on a form similar to (43). We may now proceed as for the traditional system. We write (50a) and (52) as

$$h^+ = \tilde{q}_1 - \frac{\Delta t H}{\Delta x}\delta u^+ \tag{53a}$$

$$u'^+ = \tilde{q}_2 - \frac{\Delta t g}{\Delta x}\delta h^+ \tag{53b}$$

where in $\tilde{q}_1$ and $\tilde{q}_2$ we have collected terms which depend only on values at time level t–Δt and t. Applying the operator δ( ) on (53b) and substituting in (53a) gives the Helmholtz equation

$$h^+ - \frac{\Delta t^2 g H}{(\Delta x)^2}\delta^2 h^+ = \tilde{q}_1 - \frac{\Delta t H}{\Delta x}\delta\tilde{q}_2 \tag{54}$$

where $\delta^2( ) = \delta(\delta( ))$. At the end of a time step (54) is solved to obtain h^+. Values of momentum and the velocities fields at time t=t–Δt are then computed as follows. Given h^+ we determine δu^+ using (50b). We can then calculate the new values of the momentum $(uh)^+$, from (50b), and finally compute u^+ as $u^+ = (uh)^+/h^+$.

The reason for following this procedure is that thereby we maintain conservation of mass and momentum. (50a) is satisfied because we used it to derive the Helmholtz equation from which h^+ is determined. When multiplied by Δx times a constant density ρ and then summed over all gridpoints (50a) gives that the total mass predicted by the semi-implicit system is equal to that predicted by the explicit system. Therefore as the explicit system conserves mass so must the semi-implicit. Similarly when the momentum is obtained from (50b) we can show by a summation over a gridpoints of this equation that the semi-implicit system conserves momentum.

We have derived a similar semi-implicit model for the cell-integrated energy system. The derivation is quite analogous and we end up with a Helmholtz equation which is formally equal to (54). The expression for $\tilde{q}_2$ is, however, different and instead of (50b) we have an energy equation. $\tilde{q}_2$ for the energy system becomes

$$\tilde{q}_2 = \frac{1}{UH}\left(E^+_{\exp} + \frac{1}{2}gH^2 - (\frac{1}{2}U^2 + gH)\,h^+_{\exp} - \frac{1}{2}(u'^2 h + gh'^2 + 2Uu'h')^0 \right) - \frac{\Delta t g}{\Delta x}\left(\delta u^- - 2\delta u^0 \right) \tag{55}$$

and the energy equation substituting (50b) is

$$E^{+} = E^{+}_{\exp} - \frac{\Delta t}{\Delta x}\left(gUH\left(\delta h^{+} + \delta h^{-} - 2\delta h^{0}\right) + \left(\frac{1}{2}U^{2}H + gH^{2}\right)\left(\delta u^{+} + \delta u^{-} - 2\delta u^{0}\right)\right). \quad (56)$$

Results from integrations with the two semi-implicit cell-integrated models were compared with results from corresponding traditional models. The traditional models are building upon the same basic equation systems, i.e. the momentum and the energy system. The difference from the cell-integrated models is that a traditional semi-Lagrangian formulation is used instead of the cell integrated, just as in the model derived in the beginning of this section, i.e. in (43)-(45). The derivation of the two additional traditional models proceeds completely analogous to that of the semi-implicit cell integrated models.

Using a time step Δt=2500 s, 25 times larger than that used in the explicit runs presented in Figure 3, the two cell-integrated and the three traditional semi-implicit models were integrated 44 time steps or 30.5 hours. This is the same integration time as in the explicit runs during which period the linear solution to the differential equations is moving slightly less than five times through the domain. The resulting height fields at the end of the integration period is shown on top of each other in Figure 6.

The solutions of the three traditional models are indistinguishable in the figure and appear all as the solid line. It is not yet possible to see any decrease of amplitude for these solutions and they deviate only very little from the sine shape. The cell-integrated model solutions are rather similar to the traditional solutions except for a slight damping which as for the explicit solutions can be ascribed to the choice of piecewice constant functions in grid cells when computing length-weighted values. The phase is similar for all solutions. Due to the semi-implicit time stepping the phase speed c has been reduced compared to c_g, the phase speed of the true linear solution given by (29). For all five integrations we find the same relative phase speed reduction $(c-c_g)/(c_g-U)$=-12.4%. This corresponds closely to the value computed from a solution to the linearized semi-implicit cell-integrated momentum system corresponding to (47) and (49). The phase speed for solutions to this system is found to be

$$c = U + \frac{1}{2\Delta t k}\arctan\frac{\left(\left(\cos\left(\frac{k\Delta x}{2}\right)\right)^{2} - 1\right) S}{\left(S^{2} - 1\right)\cos\left(\frac{k\Delta x}{2}\right)}, \text{ for } k\Delta x \neq \pi \quad (57)$$

where

$$S = \frac{2\Delta t\sqrt{gh}}{\Delta x}\sin\frac{k\Delta x}{2}.$$

The linearization of (47) and (49) proceeds similar to that carried out in Section 3 for the corresponding explicit system. For the value of Δt=2500 s as used in the present experiments we get from (36) that μ=0.5. This value was used in the derivation of (57). A curve for the relative phase speed $(c-U)/(c_g-U)$ determined from (57) is shown in Figure 5 as a function of $k\Delta x/\pi$. It is seen that for this large time step 2500 s, the semi-implicit scheme results in drastic reductions of the phase speed compared to that of the true linear solution, especially for short waves.

As with the explicit models the semi-implicit models were tested in integrations over 62.5 days, using again a week Robert-Asselin time filter with a coefficient equal to 0.005. The model behaved as expected. During the long integration period the initial gravity wave was damped out completely due to the time filter, the interpolations and the length-weighted mean calculations. In the cell-integrated models the mass and momentum or mass and energy were conserved exactly and in the traditional models they were not.

5. Summary and conclusions

A first main purpose of the present study was to investigate the stability of the cell-integrated semi-Lagrangian scheme. For that purpose two versions of the scheme were applied to the one-dimensional shallow water equations, a mass and momentum conserving version and a mass and energy conserving version. The one-dimensional shallow water models established are conveniently simple and at the same time they are well suited for the present study as they have gravity wave solutions the stability of which we wanted to study. In spite of the fact the models conserved mass and momentum or mass and energy exactly instabilities developed when they were integrated using the explicit leap-frog time extrapolation scheme with a time step exceeding a certain limit. The conservation properties were maintained until the time when trajectories start to cross after which the model "explodes'. The CFL condition that determines the maximum permissible time step was derived from a linearized version of the models. The instabilities were found to develop in close agreement with deductions from the linearized system.

A second main purpose of our study was to find a way by which the cell-integrated semi-La-grangian scheme could be combined with the semi-implicit time stepping. From the start this was not obviously as firstly the divergence has been eliminated and appears indirectly in the trajectory positions and secondly because some of the prognostic variables are nonlinear in

the basic variables. For both, the energy and momentum conserving versions, these difficulties were overcome and semi-implicit models were established which maintain the conservation properties. The results of test integrations with these models were compared with those obtained from traditional semi-Lagrangian semi-implicit models. Besides the usual traditional model with velocity and height as prognostic variables we also tested traditional models corresponding to the cell-integrated models in which momentum instead of velocity or energy instead of velocity was the second predictive variable. Results of short term integrations were very much similar for the different models except for a more severe damping in the cell-integrated models, due to the assumption of piecewice constant values in the grid cells. This damping could have been reduced by assuming variations within the grid cells described by higher order polynomials.

Extended integrations of the cell-integrated models demonstrated the exact fulfilment of their conservation properties whereas the traditional models neither conserved mass, momentum or energy. We have not listed the changes of mass, momentum and energy which were found in the extended integrations because these numbers clearly are not representative of the performance of the respective schemes in realistic large scale models. A result which might be generalized is, however, that among the traditional models a better conservation of energy or momentum was obtained when respectively the energy or momentum equation were chosen as a model equation.

The purpose of the test integrations performed were primarily to show that the implementation of the semi-implicit scheme in the cell-integrated systems works as satisfactory as in the traditional semi-Lagrangian models. A generalization of the combined cell-integrated semi-implicit schemes developed here to the two- and three-dimensional model formulations which were outlined in Machenhauer (1994) seems now straight forward. As usual we shall start with the development of a two-dimensional shallow water model for which useful comparisons of performance and efficiency with traditional schemes can be made.

References

Bermejo, R. and A. Staniforth, 1993: The conversion of semi-Lagrangian advection schemes to quasi-monotone schemes. Mon. Wea. Rev., **120**, 2622-2632.

Gravel, S. and A. Staniforth, 1993: A Mass-Conserving Semi-Lagrangian Scheme for the Shallow-Water Equations. Mon. Wea. Rev., **122**, 243-248.

Hirt, C. W., Amsden, A. A. and J. L. Cook, 1974: An arbitrary Lagrangian-Eulerian Computing Method for all Flow Speeds. J. Comput. Phys., **14**, 227-253.

Kwizak, M. and A. J. Robert, 1971: A semi-implicit scheme for grid point atmospheric models of the primitive meteorological equations. Mon. Wea. Rev., **99**, 32-36.

Laprise, R. and A. Planté, 1995: SLIC: A semi-Lagrangian integrated-by-cell mass conserving numerical transport scheme. Mon. Wea. Rev., **123(2)**, 553-565.

Machenhauer, B., 1994: A note on a Mass-, Energy- and Entrophy Conserving Semi-Lagrangian and Explicit Integration Scheme for the Primitive Meteorological Equations. MPI Workshop on Semi-Lagrangian Methods, Hamburg 8-9 Oct. 1992. MPI Report **146**, 73-102.

Moorthi, S., R.W. Higgins and J.R. Bates, 1994: A Global Multilevel Atmospheric Model Using a Vector Semi-Lagrangian Finite Difference Scheme. Part 2: Version with Physics. Submitted to Mon. Wea. Rev.

Priestly, A., 1993: A quasi-conservative version of the semi-Lagrangian advection scheme. Mon. Wea. Rev., **121**, 621-629.

Rancic, M., 1992: Semi-Lagrangian Piecewice Biparabolic Scheme for Two-Dimensional Horizontal Advection of a Passive Scalar. Mon. Wea. Rev., **120**, 1394-1406.

Robert, A., 1969: The integration of a spectral model of the atmosphere by the implicit method. Proc. of WMO/IUGG Symp. on NWP, Tokyo, Japan Meteorological Agency, VII.19-VII.24.

Robert, A., 1981: A stable numerical integration scheme for the primitive meteorological equations. Atmos. Ocean., **19**, 35-46.

Robert, A., 1982: A semi-Lagrangian and semi-implicit numerical integration scheme for the primitive meteorological equations. Jpn. Meteor. Soc., **60**, 319-325.

Williamson, D. L. and J. G. Olson, 1994: Climate Simulations With a Semi-Lagrangian Version of the NCAR Community Climate Model. Mon. Wea. Rev., **122**, 1594-1610.

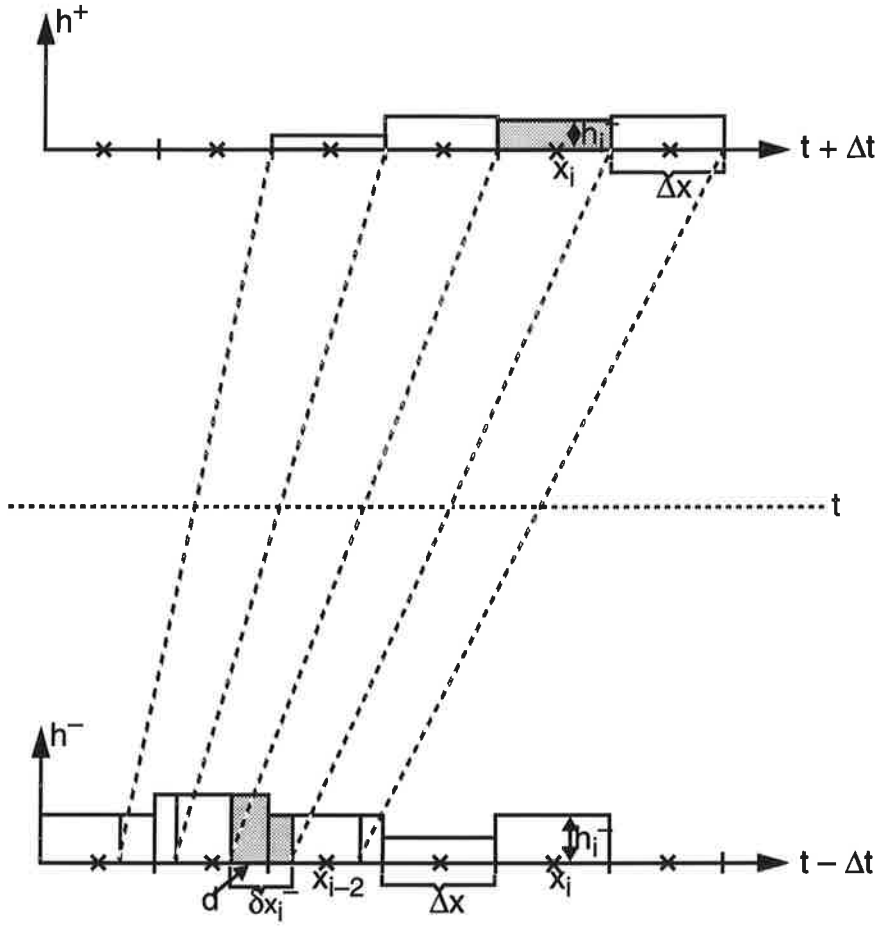

Figure 1: Schematic illustration of the Lagrangian displacement of one-dimensional cells over a time interval of 2 Δt and of quantities used in connection with the solution of the continuity equation (2).

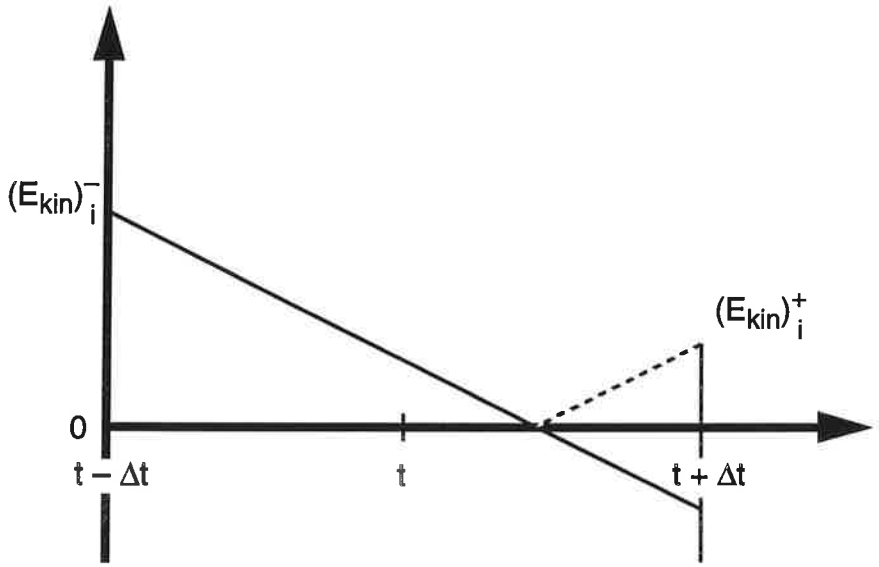

Figure 2: Schematic diagram showing the initial erroneous variation of the kinetic energy (solid line) during a time step for a cell which should change the sign of its velocity. The dashed line indicates the corrected path to the positive value adopted.

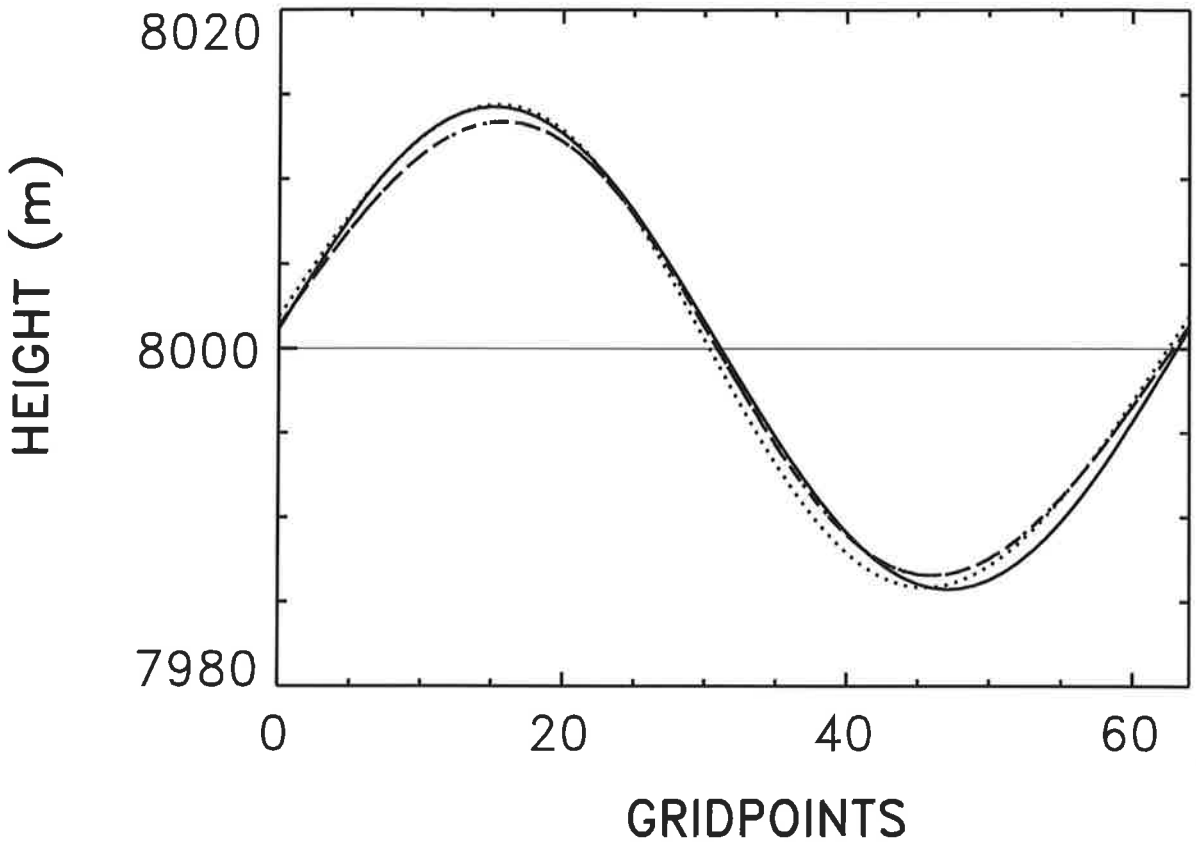

Figure 3: The height field at time t=30.5 hour for the true linear solution (solid line), and the explicit model solutions with Δt=100 s: The traditional (dotted), the cell-integrated momentum system (dashed) and the cell-integrated energy system (dot-dashed).

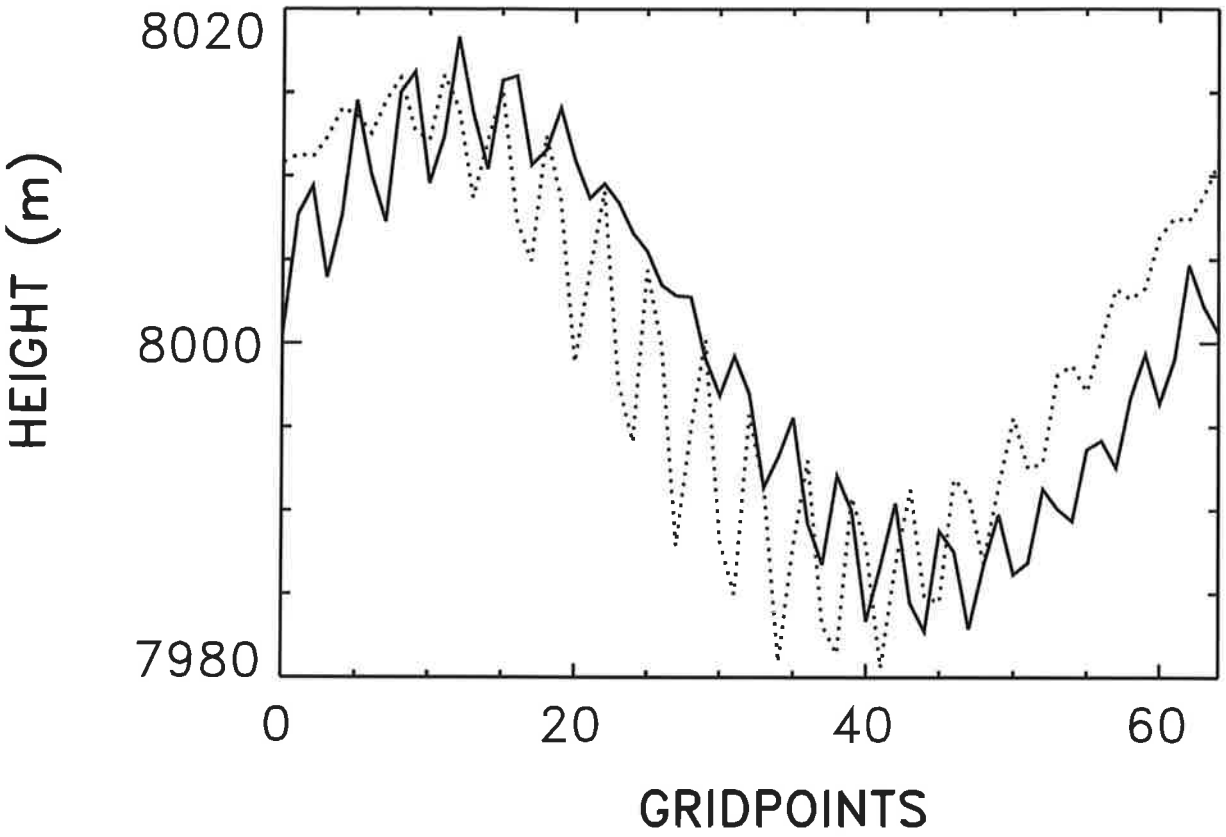

Figure 4: The height field from explicit integrations of the cell-integrated models with a time step Δt=300 s: The momentum system at t=70Δt (solid) and the energy system at t=64Δt (dotted).

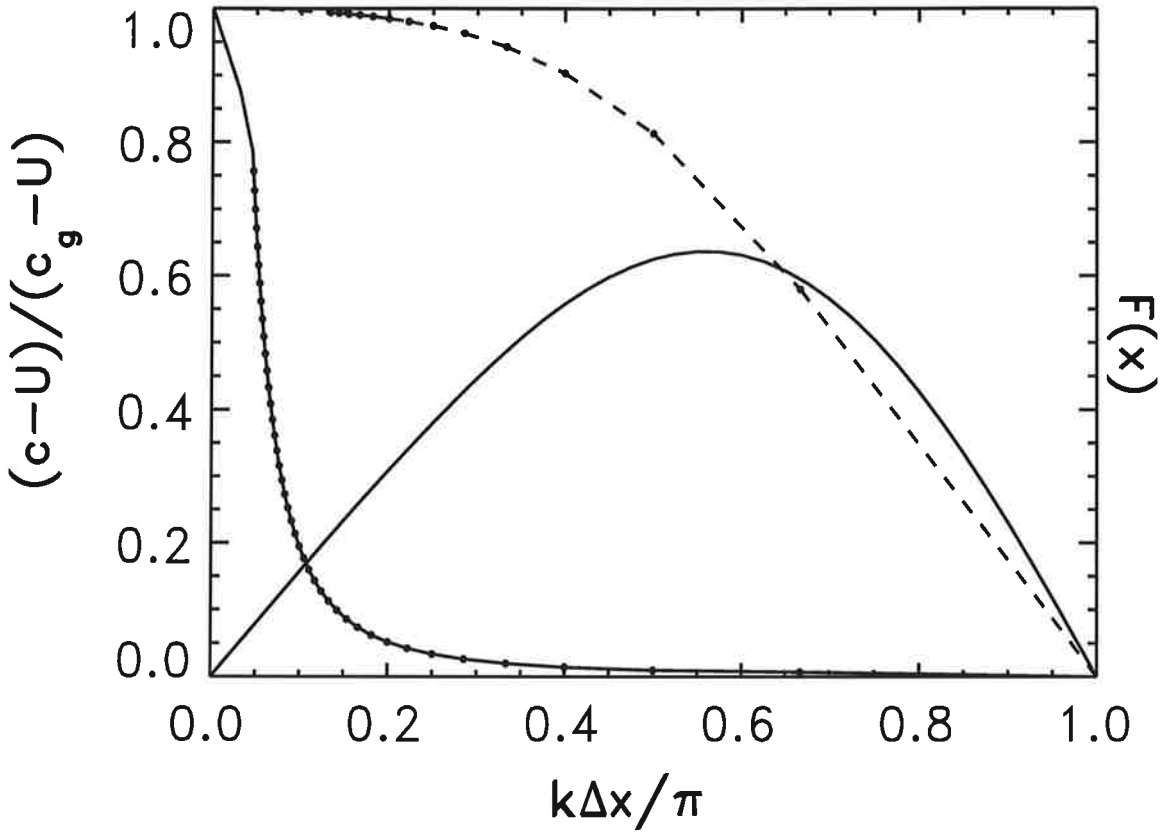

Figure 5: The relative phase speed of harmonic solutions to the linearized cell-integrated models for the explicit model (dashed), given by (39) and for the semi-implicit model with Δt=2500 s (solid), given by (57). At both curves are point marks at wave length of $3\Delta x$, $4\Delta x$, ... etc. The solid curve without dots is the function F(x) appearing in (39).

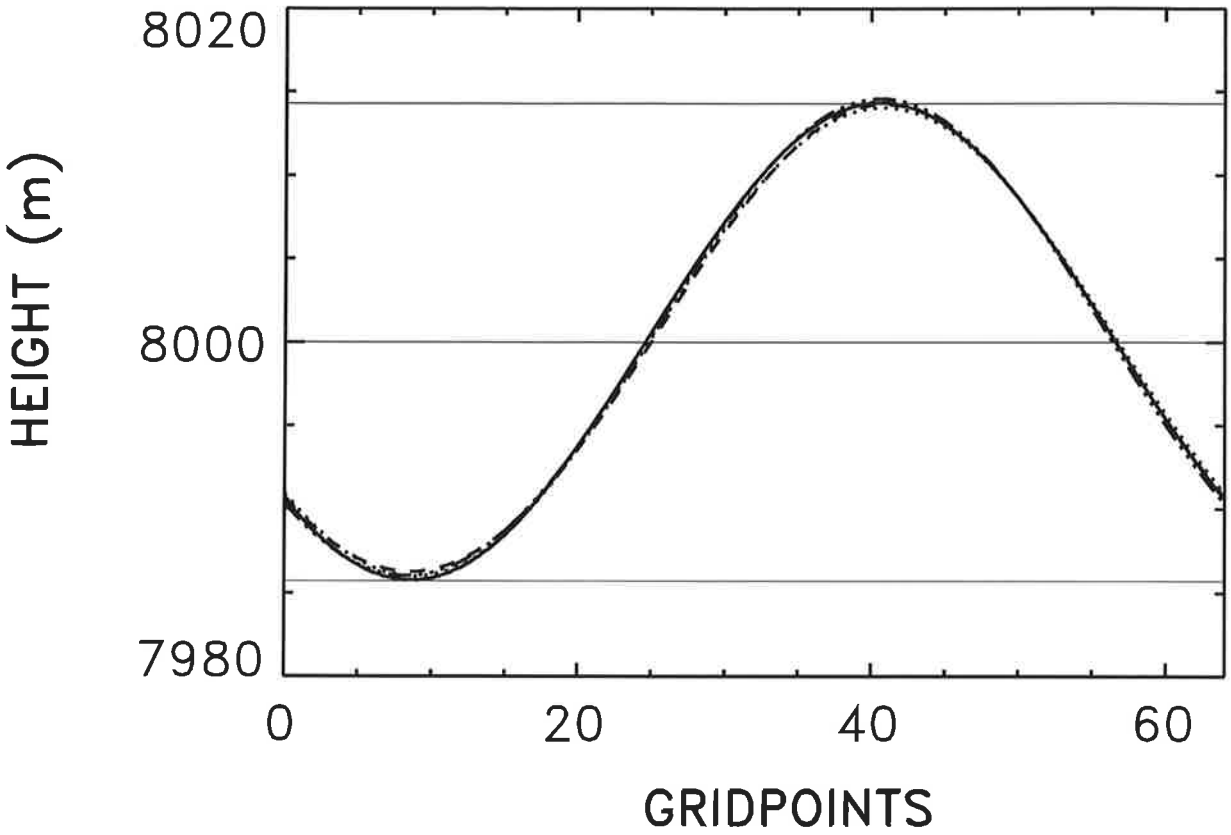

Figure 6: The height field at time t=30.5 hour for semi-implicit model solutions with Δt=2500 s: The cell-integrated momentum system (dotted), the cell-integrated energy system (long dashed), the traditional velocity system (solid), the traditional momentum system (dot-dashed) and the traditional energy system (short dashed).